한국항해항만학회지 제26권 제1호(항해항만통합권 제1호), pp.127~136, 2002 (ISSN-1598-5725)
Journal of Korean Navigation and Port Research

Design and Realization of Phase Sensitive Detector Circuitry of Two-Channel Ring-Core Flux-Gate Compass

*Jeong-Bin Yim**

**Mokpo National Maritime University Faculty of Maritime Transportation System*

2-체널 링-코어 플럭스-게이트 콤파스의 위상검출 회로 설계와 구현에 관한 연구

임 정 빈*

*목포해양대학교 교수

Abstract : *This paper presents a discussion on the design and realization for the Phase Sensitive Detector (PSD) circuitry of Flux-gate Compass that gives direction information to the Directional Frequency Analysis and Recording (DIFAR) Sonobuoy in Air Anti-Submarine Warfare. PSD circuitry is realized with Twin-T RC networked active band-pass filter. Results of a performance test for the PSD circuitry shows that the effectiveness of band-pass filtering of desired $2F_0$ second harmonic signal, which is proportional to the direction of earth's magnetic field. This resulted in the extraction of direction information.*

Key words : *Electronic Magnetic-compass, Sonobuoy, 2-axis Ring-core Flux-gate, Earth's Magnetic, Phgase Sensitive Detector(PSD)*

요 약 : 항공 대잠수함전에 사용되는 방향주파수분석저장 소노부위 (DIFAR Sonobuoy)에 방위정보를 제공하는 플럭스-게이트 콤파스의 위상감응검출 (PSD) 회로 설계와 구현에 관해서 기술하였다. PSD 회로는 쌍동-T RC 회로망을 갖는 능동형 대역필터로 구성하였다. PSD 회로에 대한 성능실험 결과, 대역통과 필터가 지구자장 방향에 비례하는 $2F_0$의 2차 고조파 신호를 효과적으로 걸러냄을 확인하였다. 그 결과 방위신호 정보를 획득할 수 있었다.

핵심용어 : 전자 마그네틱컴파스, 소노부위, 2축 링-코어 플럭스게이트, 지구자장, 위상검출기

1. INTRODUCTION

Sonobuoy is a sensor designed to relay underwater sounds, associated with ships and submarines, to remote processors. They are vital for the success of Air Anti-Submarine Warfare (ASW) [1]. There are several kinds of Sonobuoy as their purpose. In case of Directional Frequency Analysis and Recording (DIFAR) Sonobuoy, it can provide a magnetic bearing to the signals of interest with help of Flux-gate electrical compass. This feature allowed the aircrew to track and fix the location of the contact of interest objects. Thus, the Flux-gate compass is key component to measure the target bearings in underwater environments.

Traditionally, the magnetic compass has been used in navigation for centuries. Advances in technology have led to the solid state electronic compass based on Flux-gate magnetic sensor. Electronic compass offers many advantages over conventional needle type or gimbaled compass such as: shock and vibration resistance, electronic compensation for stray field effects, and direct interface to electronic navigation systems. The Flux-gate has been the workhorse of magnetic field strength instruments both on earth and in space. It is rugged, reliable, and physically small and it requires very little power to operate. These characteristics, along with its ability to measure the vector components of magnetic fields over a 0.1 nano-Tesla (nT) to 1 milli-Tesla (mT) range from DC to several kHz, make it a very versatile instrument. This sensor provide a low cost means of magnetic field detection [2],[3].

Once a Sonobuoy hits the water, it descends approximately 40~60 feet underwater until its battery is activated by the sea water. After several hours of operation, the Sonobuoy battery fails and water-soluble seals dissolve

* 종신회원, jbyim@mmu.ac.kr, 061)240-7051

which allows the Sonobuoy to sink to the bottom. Thus, Sonobuoy is expendable device that is never recovered after launched from the aircraft. This inexpensive ASW method not only considers the cost of Sonobuoy, but also the operating costs for the aircraft. Before any Sonobuoy is developed, a careful analysis is always conducted to determine the cost effectiveness versus the expected performance. An expensive Sonobuoy may perform superbly, but if it costs too much, the Navy will never be able to buy sufficient quantities. One of the possible solutions to contain costs is reducing the number of electronic components.

Generally, conventional Flux-gate compass has two isolated input circuits to sense the two sense windings of Flux-gate sensor [4],[5]. Furthermore, the differences between the two isolated input circuits caused direction error of Flux-gate compass. To cope with those problems, twin-T network based Phase Sensitive Detector (PSD) to detect direction information of Flux-gate sensor was proposed and applied to Flux-gate compass in this paper.

2. BASICS OF DIFAR SONOBUOY

There are three classes of Sonobuoy: passive, active, and special purpose. The passive Sonobuoy is commonly categorized as Low Frequency Analysis and Recording (LOFAR) and Directional Frequency Analysis and Recording (DIFAR) Sonobuoy. LOFAR Sonobuoy responds equally to sound from all directions. Thus, the direction of contact is unavailable. While, DIFAR Sonobuoy usually consists of multiple hydrophones that respond to sound from different direction with a magnetic compass. Thus, DIFAR Sonobuoy provides a magnetic bearing to the signals of interest. This feature allowed the aircrew to track and fix the location of the contact of interest objects [6].

Fig. 1 shows the schematic mechanism of DIFAR Sonobuoy. In Fig. 1, Hydrophones are to receive acoustic pressure waves and converts pressure waves to voltage. Compass is to provide magnetic reference. Transmitter is to establish high frequency radio carrier for FM transmission.

3. BASICS OF MAGNETIC SENSING

Earth's Magnetic Field

The earth's magnetic field intensity is approximately 30000 nT at the equator and 60000 nT at the poles on the surface and has a component parallel to the earth's surface that always points toward magnetic north. This is the basis for all magnetic compasses. The key words here are parallel to the earth's surface and magnetic north.

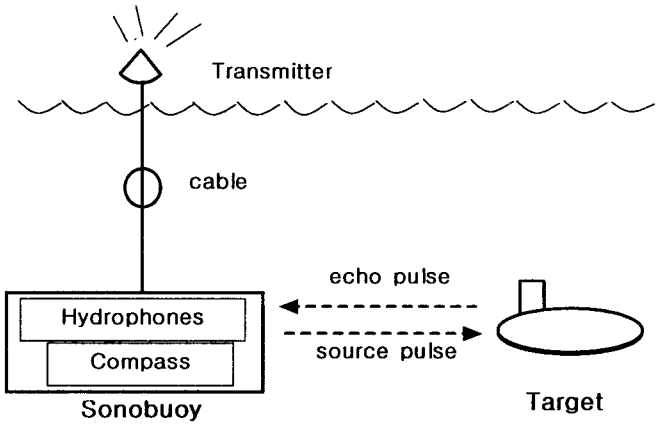

Fig. 1 Schematic mechanism of DIFAR Sonobuoy.

Fig. 2 shows how the earth's magnetic field (F_T) is composed of a vertical (F_V) and horizontal (F_H) component. The angle between the magnetic field and the horizontal component is known as *Inclination* (Ψ_I). It is well known that the earth's magnetic poles do not correspond with its geographic poles. Furthermore, the magnetic field is not perfectly uniform, it is irregular. This phenomenon is called *Variation* (Ψ_v) that is the angle between true north and the horizontal trace of the magnetic field [7].

A good compass should point toward the direction of the horizontal component of the magnetic field where the compass is located. The key for accurately finding a

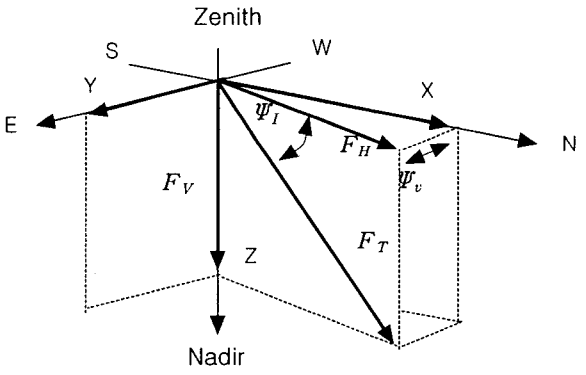

Fig. 2 Vector magnetic components: Variation (Ψ_v), Inclination (Ψ_I), Horizontal Intensity (F_H), Vertical Intensity (F_V), and Total Intensity (F_T).

compass heading, or azimuth, is to determine the Horizontal intensity F_H of the earth's magnetic field.

Measuring Magnetic Field

Today, there are several types of electronic compass: Flux-gate, Magneto-resistive, Magneto-inductive, and others. One way to classify the various magnetic sensors is by the field sensing range. Table 1 lists the various sensor technologies and illustrates the magnetic field sensing ranges [8].

A common type of magnetic sensor for navigation systems is the Flux-gate as shown in Table 1. Before discussing the principle of Flux-gate operation, it is probably best to review briefly the subject of magnetic permeability. The permeability μ of a given material is a measure of how well it serves as a path for magnetic lines of force, relative to air, which has an assigned permeability of one. Some examples of high permeability materials are listed in Table 2. The values vary with proportional make-up, heat treatment, and mechanical working of the material [9].

Table 1 Magnetic sensor technology and field ranges.

Magnetic Sensor Technology	Detectable Filed Range(Gauss)				
	10^{-8}	10^{-4}	10^{0}	10^{4}	10^{8}
Squid					
Fiber-Optic					
Optically Pumped					
Muclear Procession					
Search-Coil					
Flux-Gate					
Magnetotransistor					
Magnetodiode					
Magneto Optical Sensor					
Giant Magnetoresistive					
Hall-Efect Sensor					
Earth's Field					

Table 2. Permeability ranges for some materials.

Material	Permeability μ
Supermalloy	100,000 ~ 1,000,000
Pure iron	25,000 ~ 300,000
Mumetal	20,000 ~ 100,000
Permalloy	2,500 ~ 25,000
Cast iron	100 ~ 600

Permeability μ is the magnetic circuit analogy to electrical conductivity, and relates magnetic flux density to the magnetizing force as follows:

$$\boldsymbol{B} = \mu \boldsymbol{H} \tag{1}$$

where

$\boldsymbol{B}$ = Magnetic flux density,

μ = Permeability,

$\boldsymbol{H}$ = Magnetizing force.

Since the magnetic flux in a magnetic circuit is analogous to current $\boldsymbol{I}$ in an electrical circuit, it follows that magnetic flux density $\boldsymbol{B}$ is the parallel to electrical current density. A graphical plot of the above equation is known as the normal magnetizing curve, or B-H curve, and the permeability μ is the slope.

When a highly permeable material is introduced into a uniform magnetic field, the lines of force are drawn into the lower resistance path presented by the material as shown in Fig. 3(a). However, if the material is forced into saturation by some additional magnetizing force $\boldsymbol{H}$, the lines of flux of the external field will be relatively unaffected by the presence of the saturated material, as indicated in Fig. 3(b). The Flux-gate sensor uses of this saturation phenomenon in order to directly measure the strength of a surrounding static magnetic field.

Flux-gate Sensor

Fig. 4(a) illustrates the magnetic toroidal core with the associated windings that senses the surrounding magnetic field in a Flux-gate. A Drive Winding is wound around a Toroidal core, high-permeability magnetic core. Two Sense Windings are wound around the Toroidal core at right angles to one another to sense orthogonal components of a surrounding magnetic field [10],[11].

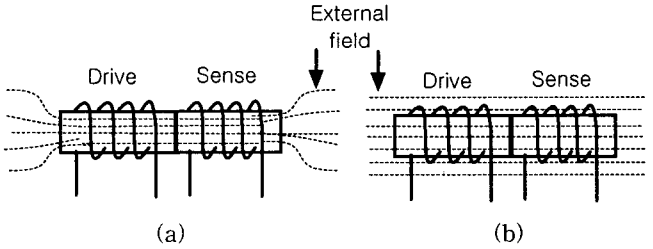

Fig. 3 External lines of flux for unsaturated core (a), and saturated core (b).

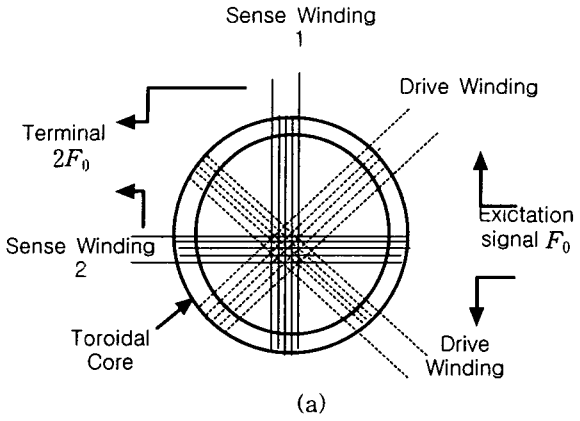

(a)

(b)

Fig. 4 Two-channel ring-core Flux-gate with toroidal excitation. Coil winding configuration (a), and real shape with a coin of 100 Korea won in the foreground for comparison (b).

In this work, the Flux-gate Compass system configured with NEXEN Company's prototype two-channel ring-core Flux-gate weighs 70 grams and draws 40mA at 8 to 18 DC voltage [12]. Fig. 4(b) shows the real shape of Flux-gate.

Fig. 5 shows fictitious wave-forms to explain the electrical operation of the two-channel ring-core Flux-gate as shown in Fig. 4. The waveform (A) is a excitation voltage applied to the Drive Winding with frequency F_0, and (B) represents induced magnetization in Sense Winding 1 and Sense Winding 2. In the absence of external magnetic filed, two Sense Windings are saturated at a same time each other as shown in (C). Thus, the net output from Terminal is to be zero. While, in the presence of an external magnetic filed, one Sense Winding saturates before the other Sense Winding saturates. The output waveforms from each of the two Sense Windings make the time difference τ as shown

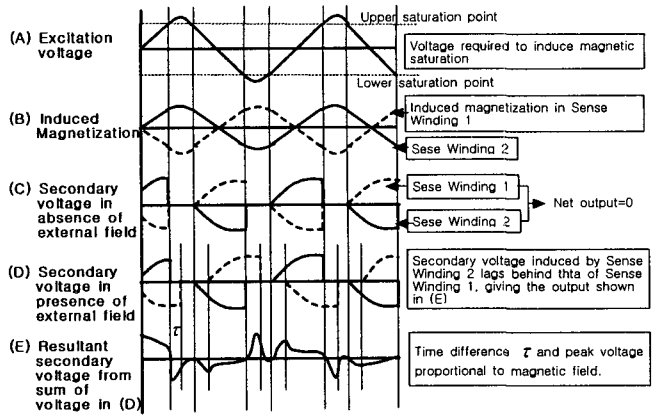

Fig. 5 Fictitious waveforms for the electrical operation of two-channel ring-core Flux-gate sensor.

in (D). The time difference τ is proportional to the phase difference $\triangle\phi$ between Sense Winding 1 and Sense Winding 2. Thus, the net output from Terminal is a pulse-like whose length and peak voltages is a function in the external magnetic field as shown in (E). The frequency of the output signal from Terminal is twice ($2F_0$) the excitation frequency (F_0) since the saturation-to-saturation transition occurs twice each excitation period.

4. CIRCUITRY REALIZATION

System Configuration

The circuitry configuration of Flux-gate compass, developed in this study, is shown in Fig. 6. It consists of Excitation Circuit (EC), Flux-gate, and Phase Sensitive Detector (PSD). As mentioned in the Fig. 1, the signal from the PSD, which is proportional to the direction of DIFAR Sonobuoy, is then fed to the DIFAR Transmitter.

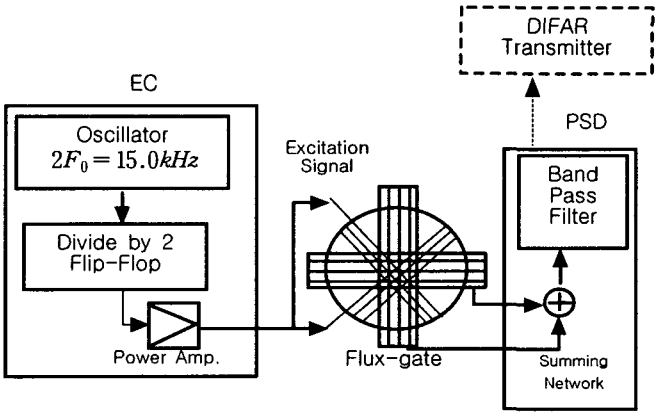

Fig. 6 Circuitry configuration for the Flux-gate compass developed in this study.

The EC consists of an Oscillator tuned to twice the excitation frequency F_0(=7.5kHz), a flip-flop (F/F) which divides the Oscillator frequency by two and a Power amplifier which is driven by the F/F and, in turn, provides the excitation current to the excitation winding. Here, The Drive Windings are driven at 7.5kHz square shaped bi-directional current pulse train, optimized to minimize the Flux-gate noise. In the presence of an external magnetic field, a second harmonic of the excitation signal is generated in the Sense Winding. The phase of Sense winding signal with respect to the Drive Winding represents the direction of the magnetic field component. The signal from the Sense Winding is then fed to a Phase Sensitive Detector (PSD).

The circuitry to the right of the Flux-gate is called the PSD, because the output is a maximum when the input signal is at the same frequency and in phase with a reference signal [13]. It detects the phase difference $\triangle\phi$ which is extracted from Summing RC network. In mechanical terms, PSD works by switching the input signal on and off at the reference frequency F_r. If the input signals are in phase (i.e., $2F_0 = F_r$), the output is a rectified version of the input signal. If they are not in phase (i.e., $2F_0 \neq F_r$), the DC output is proportional to the cosine of the phase difference. The output of this kind of phase detector is given by:

$$DC_{out} = \frac{2V_0}{\pi}\cos(\triangle\phi) \tag{2}$$

where

$\triangle\phi$ = Phase difference,

V_0 = Constant voltage in a circuit.

This type of PSD is one of a high-Q band-pass filter that amplifies frequencies only near a desired frequency (in this case $2F_0 = 15.0kHz$). In this work, twin-T networked band-pass active filter is designed and realized.

Network Design

The basic circuitry consists of two passive networks, which we will refer to as network A and network B, and an OP amp. The basic network configuration is shown in Fig. 7 with indication of the variables of two passive networks [14].

It should be noted that the OP amp is used in an inverting configuration, i.e., with its non-inverting input terminal (+) grounded. We shall call this circuit an Infinite-Gain Single-Feedback circuit (IGSF) since the OP amp that is the active element normally has very high gain, and since the feedback around it is made to a single point. To characterize the properties of the two passive networks in Fig. 7, we shall use their y-parameters [15]. For network A, we may define voltage and current variables. The relations between these variables and the y-parameters of the network are:

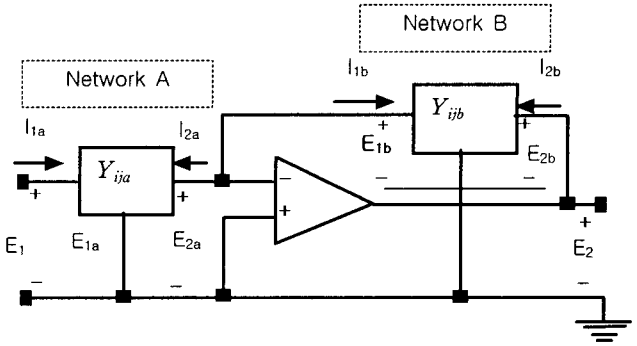

Fig. 7 The port variables for the single-feedback circuit.

$$\begin{aligned} I_{1a} &= y_{11a}E_{1a} + y_{12a}E_{2a} \\ I_{2a} &= y_{12a}E_{1a} + y_{22a}E_{2a} \end{aligned} \tag{3}$$

Similarly, for network B, the y-parameters of the network are:

$$\begin{aligned} I_{1b} &= y_{11b}E_{1b} + y_{12b}E_{2b} \\ I_{2b} &= y_{12b}E_{1b} + y_{22b}E_{2b} \end{aligned} \tag{4}$$

All of the voltage and current variables and the y-parameters defined in equations (3) and (4) are functions of $s(=\sigma+j\omega)$, the complex frequency variable. In network A, due to the virtual ground, the voltage between the inverting (-) and non-inverting (+) terminals of the OP-amp may be considered zero. Thus, the voltage E_{2a} is zero. From the second equation of (3), we see that with this condition $I_{2a} = y_{12a}E_{1a}$. In addition, since E_{1a} and E_1 are equal, we may write:

$$I_{2a} = y_{12a}E_1 \tag{5}$$

Similarly, for network B, E_{1b} is zero, and $E_{2b} = E_2$. Thus, we see that:

$$I_{1b} = y_{12b}E_2 \tag{6}$$

The virtual ground concept also tells us that the current into terminal 1 of the OP amp is negligibly small. Thus, we

see that $I_{2a}=-I_{1b}$. We may now combine equations (5) and (6) to obtain:

$$\frac{E_2}{E_1}=\frac{-y_{12a}}{y_{12b}} \tag{7}$$

The equation (7) is the open-circuit voltage transfer function for the IGSF active circuit configuration. If networks A and B are passive RC networks, their natural frequencies will be on the negative real axis of the complex frequency plane. In addition, if both of the passive networks have the some natural frequencies then the denominators of the functions y_{12a} and y_{12b} will cancel and the locations of these natural frequencies will not affect the voltage transfer function. The poles of the voltage transfer function will then be determined solely by the zeros of the transfer admittance y_{12b}.

Since a passive RC network can have the zeros of its transfer admittance anywhere on the complex frequency plane [16], we can realize complex conjugate poles in our voltage transfer function. Such poles will be restricted to the left half of the complex frequency plane for reasons of stability. Similarly, the zeros of the voltage transfer function given in equation (5) will be determined by the zeros of y_{12a}, and therefore we can realize any desired real or complex conjugate zeros. Thus, the IGSF active RC network configuration can be used to realize almost any desired pole-zero configuration.

Band-Pass Filter Realization

There are several network configurations, of which the two most common ones are the bridged-T network and the twin-T network. But the bridged-T network is not useful for producing zeros that lie close to the $j\omega$ axis. While, twin-T network has advantage that this configuration has it's pole locations determined completely by the passive networks. Thus, the pole locations will remain relatively stable and independent of changes in the active element. This is a considerable advantage when it is desired to design high-Q networks, where the poles are located close to the $j\omega$ axis, since even small pole displacements may produce instability in this case. Another advantage of this configuration is that the output impedance of the network is equal to the output impedance of the OP amp, which with high loop gain is very low [17].

If select twin-T network as network B, the transfer admittance of network A may have a single zero at the origin and a pole at -1 for band-pass network. The complete network is shown in Fig. 8.

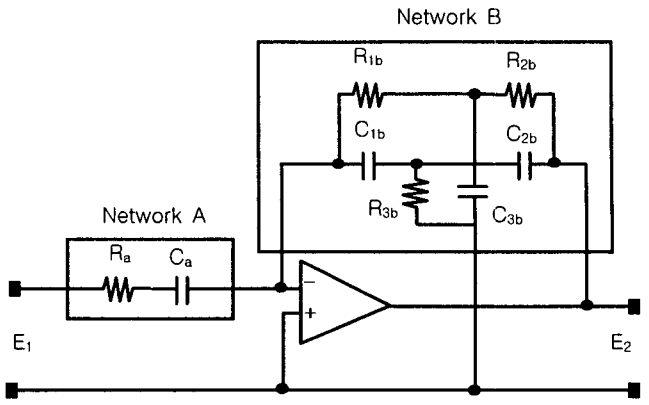

Fig. 8 Single feedback band-pass filter with networks A and B.

Here, it is a very time-consuming work to select the best design procedure and a set of many element values of capacitances and resistances in Fig. 8. Thus, in this work, the design procedures and element selections are referred to Texas Instrument's active RC network design method [18] and reference in [19]. In these references, the calculation equation to determine the RC component values are given by:

$$\begin{aligned} C_a &= H\frac{k}{2\pi f_0} \\ C_{1b} &= b\frac{k}{2\pi f_0} \\ C_{2b} &= \frac{b}{b-1}\cdot\frac{k}{2\pi f_0} \\ C_{3b} &= \frac{b^2}{(b-1)(1+a)}\cdot\frac{k}{2\pi f_0} \end{aligned} \tag{8}$$

and

$$\begin{aligned} R_a &= \frac{1}{H}\cdot\frac{1}{k} \\ R_{1b} &= \frac{1}{b}\cdot\frac{1}{k} \\ R_{2b} &= \frac{(b-1)}{b}\cdot\frac{1}{k} \\ R_{3b} &= \frac{(b-1)(a+1)}{b^2}\cdot\frac{1}{k} \end{aligned} \tag{9}$$

where

Q = Wanted quality factor,

$a=\frac{1}{Q}$,

$b=(2.5-a)\frac{1+a}{2+a}$,

$H=\frac{A_0}{Q}$,

k = Wanted impedance de-normalization constant.

The desired characteristic of band-pass filter in Flux-gate compass is $f_0 = 15.0\,kHz$, $|A_0| = 20(40dB)$, and $Q=10$. The resultant values calculated from equation (8) and (9) are:

$C_a = 1061.0\,nF$, $C_{1b} = 666.9\,nF$, $C_{2b} = 2594.8\,nF$,
$C_{3b} = 2965.1\,nF$, and
$R_a = 500.0\,k\Omega$, $R_{1b} = 795.6\,k\Omega$, $R_{2b} = 204.5\,k\Omega$,
$R_{3b} = 178.9\,k\Omega$, where, $k = 10^{-5}$.

As mentioned in the introduction, possibly small size of elements is required to cut the costs of Flux-gate compass. To comply with this requirement, the impedance de-normalization constant was choose as $k=10^{-5}$. This value was determined by heuristic method with number of iteration calculation.

5. EXPERIMENTS & DISCUSSIONS

Test Procedures

Fig. 9 shows test environment set-up in a normal room without any electrical interference shielding. The Flux-gate compass circuitry is tested with the basic procedure as following:

(1) Position the Flux-gate compass at its intended location, and measure the time difference T_{diff} between phase difference $\triangle\phi$ from PSD and excitation signal as reference ones.

(2) Repeat $T_{diff}(l)$ measurement at equally spaced angle $\Theta(l)$ as,

$$\Theta(l) = \frac{360}{(L+1)} \times l \ (degree) \tag{10}$$

where
$l = 0, 1, 2, \ldots, L-1, L$,
L =Interval number of equally spaced angle.

(3) Repeat $T_{diff}(l)$ measurement with M'th iteration and get the average $\overline{T_{diff}}(l)$, then translate $\overline{T_{diff}}(l)$ into average direction $\overline{\theta_{diff}}(l)$ as,

Fig. 9 Test environment set-up in a normal room. Realized Flux-gate compass circuitry (below front), Oscilloscope with 100MHz resolution (top left), and Power supply (top right).

$$\overline{\theta_{diff}}(l) = \frac{\overline{T_{diff}}(l)}{T_{exit}} \times 360\,(degree) \tag{11}$$

where

$$\overline{T_{diff}}(l) = \frac{\sum_{i=1}^{M} T_{diff}(l)}{M} \tag{12}$$

M = Iteration number.

Measurements

A principal 8-point measurement method that is one of the conventional magnetic compass calibration techniques is introduced in the Flux-gate compass performance tests [20]. Thus, let $L=7$; $\Theta(0)=0^0$, $\Theta(1)=45^0,\ldots,\Theta(7)=315^0$ in equation (10). The test results of Flux-gate compass are shown in Fig. 10. The time differences T_{diff} between phase difference $\triangle\phi$ from PSD and excitation signal are almost proportional to the equally spaced measurement angle. These results show the magnetic field sensitive effectiveness of Flux-gate compass.

Table 3 represents the calculation results of average compass direction $\overline{\theta_{diff}}$ from the average time difference $\overline{T_{diff}}$, and the differences between given angle and $\overline{\theta_{diff}}$, called compass error e_θ. The interpolated error plots versus given angle shows in Fig. 11.

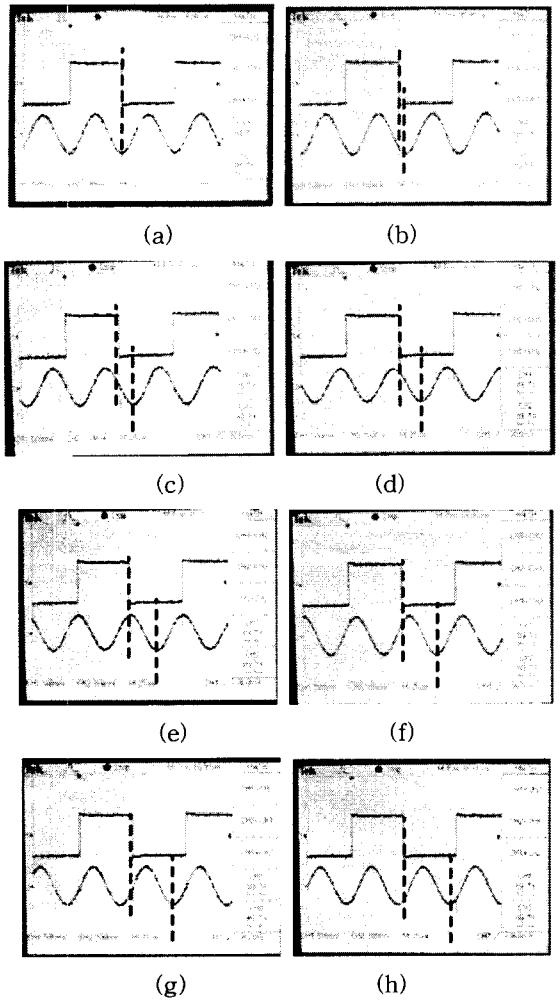

Fig. 10. Test results of Flux-gate compass. The time difference T_{diff} between phase difference $\triangle\phi$ from PSD (below at each box) and excitation signal (above at each box) are measured at 000^0(a), 045^0(b), 090^0(c), 135^0(d), 180^0(e), 225^0(f), 270^0(g), 315^0(h). The two vertical dotted lines are indicating differences between the two waveforms at each box.

Table 3 The calculation results of $\overline{\theta_{diff}}$ from $\overline{T_{diff}}$, and error e_θ.

Angle	$\overline{T_{diff}}$ (μ sec.)	$\overline{\theta_{diff}}$	e_θ
0°	0	0.0°	0.0°
45°	9	48.6°	+3.6°
90°	17	91.8°	+1.8°
135°	25	135.0°	+0.0°
180°	34	183.6°	+3.6°
225°	43	230.2°	+7.2°
270°	50	270.0°	+0.0°
315°	59	318.6°	+3.6°

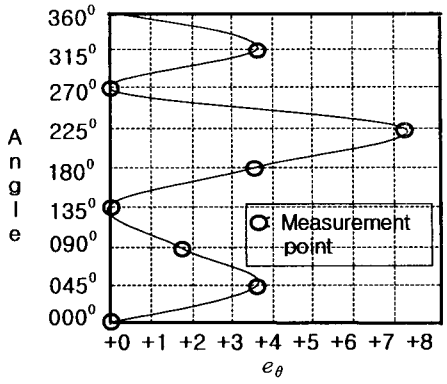

Fig. 11. Error plots versus given angle.

In Table 3, average compass directions $\overline{\theta_{diff}}$ are almost proportional to given angles. These results show that the ability of direction information extraction of the Flux-gate compass with proposed PSD in this work.

Error Analysis

In Fig. 11, the compass error is less than $+3.6^0$ except $+7.2^0$ at location 225^0. When apply the error offset values $-e_\theta$ to the average compass directions $\overline{\theta_{diff}}$, the compass errors in Fig. 11 are totally eliminated only if the magnetic interference is constant. But, the compass error varied with the change of test environments such as test location and onboard components.

This compass error is due to the magnetic interference arisen from the electric cables and other onboard components in a open area. When a compass is operating in the absence of any ferrous metals there is no distortion effects on the earth's magnetic field. In reality, compasses are mounted in vehicles, aircraft, and platforms that most likely have ferrous materials nearby. The effect of ferrous metals (iron, nickel, steel, cobalt) will distort or bend the earth's field which will alter the compass heading.

Thus, more accurate error analysis and automatic compensation techniques with proposed PSD are required to use one of the navigation magnetic compass. These analysis and techniques are beyond the scope of this study, the error problems are remained as a further works.

6. CONCLUSIONS

The design and realization procedures to implement Phase Sensitive Detector (PSD) of Flux-gate compass that

fit to the DIFAR Sonobuoy are presented. An examination of the performance of the Flux-gate compass has been shown. The design method of twin-T networked band-pass filter circuitry for the PSD and possible solutions have been developed in this work. The results are as follows:

(1) The PSD filtered only near the phase difference frequency $2F_0$ between sense windings in Flux-gate. This resulted in the extraction of useful direction information from Flux-gate sensor.

(2) The PSD have the capability of summing signals at the input. Thus, the circuitry configuration of Flux-gate compass is very simple compared with conventional PSD that have two isolated input circuits to sense the two sense windings of Flux-gate sensor.

(3) The pole location of twin-T networked band-pass filter determined completely by the passive networks. Thus, the pole locations will remain relatively stable and independent of changes in the active element.

(4) The output impedance of twin-T network is equal to the output impedance of the operational amplifier. Thus, this circuit is fit to drive other networks of DIFAR Sonobuoy, without the need for an isolating stage, and without appreciable change in the circuit characteristics due to loading.

REFERENCES

[1] Department of the USA Navy, *Technical Manual for SONOBUOYS, Basic Introduction to Air ASW Acoustic Systems*, NAVAIR 28-SSQ-500-4, Direction of Commander, Naval Air Systems Command, Jan. 15, 1994.

[2] Erik B Pedersen, Fritz Primdahl, Jan R. Pertersen, J.M.G. Merayo, Peter Brauer and O.V. Nielsen, "Digital Fluxgate Magnetometer for the Astrid-2 Satellite," *Meas. Sci. Technol. 10*, 1999, N124-129.

[3] H.J. Wieringa, *MEG, EEG and the Integration with Magnetic Resonance Images*, 1993. White papers at http://www.neuro.com/megeeg/contents.htm.

[4] Lauro Ojeda and Johann Borenstein, "Experimental Results with the KVH C-100 Fluxgate Compass in Mobile Robots," *Proc. of the IASTED International Conference Robotics and Applications 2000*, Aug. 14-16, 2000, Honolulu, Hawaii, USA.

[5] Christoph Majer, Shoji Kawahito, Michael Schneider, Martin Zimmermann and Henry Baltes, "2D Magnetic Micro Fluxgate System with Digital Signal Output," *1999 IEEE International Solid-State Circuits Conference*, TA 7.1.

[6] The Department of US Navy, *Background of Air ASW Sensors*, Oct. 30, 2001. White paper at http://sonobuoy.crane.navy.mil/sensors.htm.

[7] KVH Industries, Inc., *Overview of Compass Technology*, White paper at http://www.kvh.com/support/product_docs/oemcomov.pdf.

[8] Michael J. Caruo, Tamara Bratland, Carl H. Smith and Robert Schneider, *A New Perspective on Magnetic Field Sensing*, Honeywell, SSEC, USA. White paper at http://www.ssec.honeywell.com.

[9] Kristin L. Makovec, *A Nonlinear Magnetic Controller for Three-Axis Stability of Nanosatellites*, Master's thesis, Virginia Polytechnic Institute and State University, USA, Jul. 23, 2001.

[10] United States Patent No. 4,277,751, *Low-Power Magnetometer Circuit with Constant Current Drive*, Jul. 7, 1981.

[11] United States Patent No. 4,677,381, *Flux-Gate Sensor Electrical Drive Method and Circuit*, Jun. 30, 1987.

[12] NEXEN Company in Korea. http://www.enexen.com.

[13] Paul Shockman, *Phase Lock Loop General Operations*, AND8040/D, ON Semiconductor Components Industries, April 2001. White paper at http://www.onsemi.com

[14] 장세훈 외 3인 공저, *최신 회로망이론*, 청문각, 서울, pp.323-327, 1994.

[15] Franklin F. Kuo, *Network Analysis and Synthesis*, John Wiley & Sons, Inc., pp.253-364, 1965.

[16] Martin S. Roden, *Analog and Digital Communication Systems*, Prentice-Hall, Inc., New Jersey, pp.101-105, 1985.

[17] Randall L. Geiger and Aram Budak, "Design of Active Filters Independent of First- and Second-Order Operational Amplifier Time Constant Effects," *IEEE Trans. Circuits Sys.*, Vol. CAS-28, No. 8, pp.749-757, Aug. 1981.

[18] Texas Instrument, *Handbook of Operational Amplifier Active RC Networks*, SBOA093A, Oct. 2001. http://www-s.ti.com/sc/psheets/sboa093a/sboa093a.pdf.

[19] Maureen A. O'Leary, *Imaging with Diffuse Piioton Density Waves*, Doctor's thesis, University of Pennsylvania, USA, Chapter 3, 1996.

[20] 임정빈, *학습지침서 항해계기학*, 해군사관학교, pp.121-124. 1995.

원고접수일 : 2002년 01월 31일
원고채택일 : 2002년 03월 18일